Printed Nonfullerene Organic Solar Cells with the Highest Efficiency of 9.5%

Yuanbao Lin, Yingzhi Jin, Sheng Dong, Wenhao Zheng, Junyu Yang, Alei Liu, Feng Liu, Yufeng Jiang, Thomas P. Russell, Fengling Zhang, Fei Huang and Lintao Hou

Lin, Y., Jin, Y., Dong, S., Zheng, W., Yang, J., Liu, A., Liu, F., Jiang, Y., Russell, T. P., Zhang, F., Huang, F., Hou, L., (2018), Printed Nonfullerene Organic Solar Cells with the Highest Efficiency of 9.5%, *ADVANCED ENERGY MATERIALS*, 8(13), 1701942. https://doi.org/10.1002/aenm.201701942

Original publication available at:
https://doi.org/10.1002/aenm.201701942

WILEY-VCH

DOI: 10.1002/((please add manuscript number))

Article type: Communication

Printed Nonfullerene Organic Solar Cells with the Highest Efficiency of 9.5%

Yuanbao Lin, Yingzhi Jin, Sheng Dong, Wenhao Zheng, Junyu Yang, Alei Liu, Feng Liu, Yufeng Jiang, Thomas P. Russell, Fengling Zhang,* Fei Huang, and Lintao Hou**

Y. Lin, W. Zheng, J. Yang, A. Liu, Prof. F. Zhang, Prof. L. Hou

Siyuan Laboratory

Guangzhou Key Laboratory of Vacuum Coating Technologies and New Energy Materials

Guangdong Provincial Key Laboratory of Optical Fiber Sensing and Communications

Physics Department

Jinan University, Guangzhou 510632, P.R. China

Email: thlt@jnu.edu.cn

Y. Jin, Prof. F. Zhang

Biomolecular and Organic Electronics, Department of Physics, Chemistry and Biology (IFM)

Linköping University SE-581 83, Linköping, Sweden

Email: fengling.zhang@liu.se

S. Dong, Prof. F. Huang

Institute of Polymer Optoelectronic Materials and Devices

State Key Laboratory of Luminescent Materials and Devices

South China University of Technology, Guangzhou 510640, P. R. China

Prof. F. Liu

Department of Physics and Astronomy

Shanghai Jiao Tong University, Shanghai 200240, P. R. China

Email: fengliu82@sjtu.edu.cn

Y. Jiang, Prof. T. P. Russell

Materials Sciences Division, Lawrence Berkeley National Laboratory, Berkeley, California 94720, United States

Keywords: doctor-blading nonfullerence organic solar cell, highest efficiency, large-area ITO-free flexible structure, processing additive, morphology

Abstract

The current work reports a high power conversion efficiency (PCE) of 9.54% achieved with nonfullerene organic solar cells (OSCs) based on PTB7-Th donor and ITIC acceptor fabricated by doctor-blade printing, which is the highest efficiency ever reported in printed nonfullerene OSCs. Furthermore, a high PCE of 7.6% is realized in flexible large-area (2.03 cm^2) ITO-free doctor-bladed nonfullerene OSCs, which is higher than that (5.86%) of the spin-coated counterpart. To understand the mechanism of the performance enhancement with doctor-blade printing, the morphology, crystallinity, charge recombination and transport of the active layers are investigated. These results suggest that the good performance of the doctor-blade OSCs is attributed to a favorable nanoscale phase separation by incorporating 0.6 vol% DIO that prolongs the dynamic drying time of doctor-bladed active layer and contributes to the migration of ITIC molecules in the drying process. High PCE obtained in the flexible large-area ITO-free doctor-bladed nonfullerene OSCs indicates the feasibility of doctor-blade printing in large-scale fullerene-free OSC manufacturing. For the first time, the open-circuit voltage is increased by 0.1 V when adding 1 vol% solvent additive, due to the vertical segregation of ITIC molecules during solvent evaporation.

Solution processed bulk heterojunction (BHJ) organic solar cells (OSCs) with the potential of short payback time are good candidates to harvest solar energy for sustainable development.[1-4] The power conversion efficiencies (PCEs) of OSCs have surpassed 13%, suggesting the feasibility of commercialization in the near future.[5-7] However, most high-performance OSCs are fabricated in an inert atmosphere with spin-coating method through labor-intensive testing on small-area rigid substrates because the performance is sensitive to both size and morphology of the active layer. Generally, the performance of OSCs decreases with the area increase of the active layer, which is governed by preparing conditions such as solvents, concentration and film coating techniques. Spin-coating technique, commonly used for lab-size OSCs (< 1 cm^2), is not compatible with large-area mass-production.[8-9] Therefore, developing large-area printing technique is urgent to manufacture energy-efficient, high-throughput, low-cost and low carbon-footprint OSCs.[10] Doctor-blading is intensively used as a fully scalable, robust and reproducible technique in active layer deposition because it can be employed in sheet-to-sheet and roll-to-roll (R2R) large-area solution processing with low solution consumption, with high film homogeneity and good device performance on a flexible substrate.[11-15] For example, the comparable PCEs of fullerene-based OSCs prepared by doctor-blading and spin-coating techniques were reported by Zhao *et al*.[16] The OSCs based on poly[4,8-bis[5-(2-ethylhexyl)-2-thienyl] benzo[1,2-b:4,5-b′]dithiophene-*alt*-(4-(2-ethylhexyl)-3-fluorothieno[3,4-b]thiophene-)-2-carboxylate-2-6-diyl)] (PTB7-Th):[6,6]-phenyl-C_{71}-butyric acid methyl ester ($PC_{71}BM$) processed by doctor-blading demonstrated slightly higher PCE of 8.31% than 8.07% by spin-coating.[17] These results show that comparable or even higher performance can be realized in fullerene-based OSCs using doctor-blading by optimizing process parameters.[10]

More recently, nonfullerene (NF) acceptor has attracted much attention because of the easily tunable molecular energy level, excellent optical absorption property and low-cost potential compared to fullerene derivatives.[18] Higher PCEs over 10% in NF-based OSCs

than fullerene-based OSCs are achieved, employing 3,9-bis(2-methylene-(3-(1,1-dicyanomethylene)-indanone))-5,5,11,11-tetrakis(4-hexylphenyl)-dithieno[2,3-*d*:2′,3′-*d*′]-*s*-indaceno[1,2-*b*:5,6-*b*′]dithiophene) (ITIC) as an acceptor.[19-20] However, the high performance of fullerene-free devices is only achieved by spin-coating on small expensive rigid ITO substrates, which is incompatible with large-area R2R manufacturing. Therefore, more attention should be paid on the R2R compatible printing technique such as doctor-blading for the NF system.[13, 21] So far, the device performance of blade-coated NF OSC is still low (< 5%).[22-23] For example, Diao *et al*. reported NF OSCs by doctor-blading with a PCE of 3.2%[24] and Gu *et al*. reported R2R NF-based solar cells by slot-die with a PCE of 5%.[25] The lower efficiency of blade-printed NF OSCs than those of the state-of-the-art spin-coating ones motivates us to explore an approach to realize high-efficiency fullerene-free OSCs processed with a R2R compatible doctor-blading technique.

Here we present high PCEs of 9.54% and 7.6% achieved in doctor-blade inverted nonfullerene OSCs and flexbile large-area (2.03 cm^2) ITO-free ones based on PTB7-Th and ITIC, respectively, assisted by adding 0.6% processing additive DIO. Encouragingly, the PCEs of the small area OSCs are slightly higher than that of spin-coating ones (9.31%) and the PCEs of flexbile large-area (2.03 cm^2) ITO-free ones are even higher than that of the spin-coated counterpart (5.86%). Studies reveal that DIO facilitates the migration of ITIC molecules in doctor-bladed active layers resulting in favorable morphologies for charge generation and transportation.

The molecular structures of the electron donor PTB7-Th and acceptor ITIC used in this study are presented in **Figure 1**a. An optimized blend of PTB7-Th:ITIC (1:1.3, w:w) was used as the active layer,[26] which is processed by a doctor-blading technique illustrated in Figure 1b. Inverted NF OSCs on rigid ITO and flexible ITO-free substrates are fabricated from chlorobenzene (CB) with/without 1,8-diiodooctane (DIO) with device architectures of

glass/ITO/ZnO/BHJ/MoO_3/Ag and PET/Ag/TiO_x/BHJ/PEDOT:PSS as shown in Figure 1c, respectively.

The doctor-blading parameters like the angle of attack (90°), gap height (20 μm) and blading speed (45 mm/s) are described in the previous reference.[10] To find the optimal processing parameters, the NF OSCs with different photoactive film thicknesses (80–160 nm) are fabricated at various substrate temperatures (25–85 °C) and DIO volumes (0–1.0 vol%). The current density-voltage (*J*–*V*) characterizations of above NF OSCs are recorded in Figure S1–S3 and the corresponding photovoltaic parameters are summarized in Table S1–S3. The photovoltaic parameters of three representative NF OSCs with a thickness of 120 nm prepared under 70 °C with 0, 0.6 and 1 vol% DIO are presented in **Table 1**. The following discussion will only focus on these three representative devices with 0, 0.6 and 1 vol% DIO. In Table 1, we can see that the device incorporating 0.6 vol% DIO exhibits a remarkable PCE of 9.54%, a moderate V_{oc} of 0.83 V and a short-circuit current density (J_{sc}) of 16.0 mA/cm^2 as well as a decent fill factor (FF) of 0.71. To the best of our knowledge, a PCE of 9.54% is the highest value ever reported in single-junction NF OSCs fabricated with the doctor-blade printing. The referenced OSC without DIO shows a PCE of 7.47%, with a low V_{oc} of 0.79 V, a J_{sc} of 15.3 mA/cm^2 and a FF of 0.62; while adding 1.0% DIO also results in a low PCE of 4.79% with a J_{sc} of 11.5 mA/cm^2 and a FF of 0.47, but a large V_{oc} of 0.89 V. Thus it can be concluded that DIO pronouncedly impacts the performance of doctor-blading NF devices. Furthermore, statistical PCEs and V_{oc} dependences on DIO volume are shown in **Figure 2**a. The V_{oc} of doctor-bladed PTB7-Th:ITIC OSCs increases from 0.79 to 0.89 V with the DIO volume variation from 0 to 1 vol%. The big increase of 100 mV in V_{oc} has not been reported in NF OSCs with a tiny amount of DIO addition.

To compare the difference between doctor blading and spin coating, another controlled sample is fabricated by spin-coating under the same conditions (shown in Figure 2b and Table 1). The optimal performance of doctor-bladed OSC is superior than the controlled spin-

coating one with a PCE of 9.31%, indicating the effectiveness of doctor-blading technique in production of NF OSCs. In addition, it should also be pointed out that ITO requires highly energy-intensive processing bearing more than 70% cost in the production of an OSC module, which is a major impediment to lower material and processing expense of OSCs.[27-28] Therefore, to reduce the cost of OSCs, efficient large-area flexible ITO-free devices must be developed, which can be easily achieved with blade-coating than spin-coating. Encouragingly, the large-area (2.03 cm^2) flexible ITO-free NF OSC with doctor-blade printing exhibits a remarkable PCE of 7.6%, which is the highest PCE reported to date in large-area flexible ITO-free doctor-bladed NF OSCs. The decreased J_{sc} (14.7 mA/cm^2) and V_{oc} (0.81 V) in ITO-free doctor-bladed OSCs should be mainly attributed to the lower conductivity of the PEDOT:PSS layer than ITO (760 S/cm vs. 3400 S/cm).[29] In comparison, a low PCE of 5.86% is obtained in the flexible ITO-free spin-coated OSC (consuming four times more solution than the blade-coated one), which illustrates great benefits of doctor-blade printing for low-cost NF OSC manufacturing.

As presented in Figure 2c, the PCEs of both small-area and large-area NF OSCs fabricated by doctor-blade printing are the highest values among previous printed NF OSCs reported to date, which also catch up to the representative printed fullerence OSCs.[23-25, 29-32]

To understand the function of DIO in PTB7-Th:ITIC BHJ formed by doctor-blading, we utilize a transient monitoring technique to track the drying processes of the three NF blend films (see Figure S5). The final drying time is about 72, 506 and 1189 s for doctor-bladed films on the substrates at 70 °C with 0, 0.6 and 1 vol% DIO, respectively. The final drying time of the film from pure CB (boiling point: 131 °C) is much shorter than those of films from CB:DIO, indicating that adding a tiny small volume of DIO (boiling point: 332 °C) can prolong the drying time and thus strongly affect the final morphology of active films, which determines the exciton diffusion, dissociation, bimolecular recombination and free charge transport efficiency.[10]

Grazing incidence X-ray diffraction (GIXD) was used to investigate the structure order of doctor-bladed active thin films which are presented in **Figure 3**. As seen in 2-D diffraction images (Figure 3a), thin film processed without DIO showed quite broad scattering peaks. The (100) peak located at ~ 0.3 A^{-1} is quite broad and composed of both PTB7-Th and ITIC lamellar packing features. The π-π stacking is more pronounced in out-of-plane direction, which located at ~ 1.67 A^{-1}. The π-π stacking is thus also constituted of both material features since the π-π stacking of PTB7-Th is located at 1.60 A^{-1}. BHJ mixtures blade-printed from 0.6 vol% DIO showed quite strong scattering signals. A series of peaks are seen in in-plane direction (Figure 3b), which come from the polymorphic crystalline structure of ITIC. PTB7-Th (100) diffraction peak can be clearly noted at 0.26 A^{-1}. Diffraction peaks at 0.31, 0.36, 0.43 A^{-1} come from different packing motifs of ITIC, and corresponding second ordered peaks can be seen in higher q range.[33] A strong diffraction peak at 0.50 A^{-1} is seen in out-of-plane direction, coming from other ITIC packing structure. The π-π stacking of ITIC is seen in out-of-plane direction, which is also splitted into two peaks (one located at 1.55 A^{-1} and another located at 1.69 A^{-1}). We currently cannot well separate out the polymorphic structure of ITIC crystals. However, it is quite obvious the film crystallinity changed drastically. 1% DIO processed BHJ thin film showed quite similar crystalline order comparing to 0.6% DIO thin film, and thus the difference in device performance should come from other origins rather than crystalline order.

Resonant soft X-ray scattering (RSoXS) was employed to probe the length scale of phase separation of these blade-coated thin films (Figure 3c). 285.2 eV photon energy was used in the experiment. It is seen that thin film coated without DIO showed a quite weak phase separation, with a quite low intensity scattering hump around 0.01 A^{-1}, corresponding to a distance of ~ 60 nm. Adding 0.6 vol% of DIO improved the RSoXS intensity, and the scattering hump shifted to 0.0068 A^{-1}, giving a distance of phase separation of ~90 nm. Film

processed using 1 vol% of DIO showed a similar phase separation with 0.6 vol% case and a slightly higher intensity, which thus cannot explain the lowered device performances.

Transmission electron microscopy (TEM) was employed to examine the phase image of BHJ thin films and images are presented in **Figure 4**a-c. The TEM image of the film without DIO (Figure 4a) shows some aggregated domains and a weak fibril network structure. When 0.6 vol% DIO is used (Figure 4b), BHJ thin film exhibits a more refined fibril network, and aggregated domains disappeared. Such a morphology gives rise to improved J_{sc} and FF. 1 vol% DIO processed thin film showed a similar TEM result (Figure 4c) with 0.6 vol% DIO case. Cross-section scanning electron microscopy (SEM) was used to image vertical segregation of BHJ thin films (Figure 4d-f). In general, all these thin films showed a homogeneous morphology. It is noticeable that there are some small granular aggregates (10-20 nm) in BHJ without DIO (Figure 4d), which is consistent with TEM image in Figure 4a. Finer nanoscale cross-sectional morphology can be observed in BHJ with 0.6 vol% and 1 vol% DIO processed samples (Figure 4e-f). Thus it is still difficult to find the direct correlation of morphology to device performances for 0.6 vol% and 1 vol% processing conditions. While in both cases we clearly see fibril type network, it is thus suspected the internal structure inside the mesh network is different.

We carried out the photoluminescence (PL) measurement of neat PTB7-Th, ITIC and three blend films and these results are presented in **Figure 5**a. The neat PTB7-Th and ITIC films showed distinctive PL spectra. Thin film processed without DIO showed a suppressed PL spectrum with the similar PL peak position to that of ITIC. Thus PTB7-Th and ITIC can form good mixtures. And although PTB7-Th shows crystalline nature, those entities are quite small and are surrounded by ITIC rich domains to quench its PL. We see nanometer aggregates of them in 0% DIO processed thin film in TEM, and these species are well above the exciton diffusion length and thus should account for the residual film PL. When 0.6 vol% DIO is used, PL is fully quenched, and thus the BHJ film is much better mixed, which agrees

well with morphology characterizations. The nano sized phase separation in a well-developed morphology accounted for the good device performance. When 1 vol% DIO is used, the PL slightly grows up with the blue shift of peak, indicating the formation of large sized ITIC crystallites. Thus in-between the fibrils, the formation of ITIC crystals could lead to a decrease of ITIC concentration, which reduces electron conductivity and leads to a low device performance. These observations are further supported by electroluminescence (EL) investigations.[34-35] The EL spectra of the devices based on neat PTB7-Th, ITIC and blends were recorded and shown in Figure 5b. New shoulders at around 1000 nm are seen in BHJ blends, which come from the donor/acceptor (D/A) charge transfer (CT) radiative recombination. 0 vol% DIO processed thin film showed a moderate CT emission; 0.6 vol% DIO processed thin film showed a relative high CT emission; 1 vol% DIO processed thin film showed a low CT emission as well as the ITIC emission at ~770 nm. Thus the quality of mixing is the best in 0.6 vol% DIO processed thin film due to the easy detectability of CT emission with fine D/A phase separation interfaces.[34] The ITIC emission in 1 vol% DIO case indicates there is no efficient energy transfer from ITIC crystallites to mixed domains to quench its EL. And thus these ITIC crystallites should be bleached out from mixed regions into a more polymer rich domain, which reduce carrier transport ability and device fill factor. Furthermore, we directly probed the CT absorption by a sensitive Fourier-transform photocurrent spectroscopy (FTPS) technique, as shown in Figure S6. The relevant interfacial molecular parameters can be extracted by fitting the low energy region.[36-37] The reorganization energy is 0.18 eV for 0.6 vol% DIO OSC, whereas it is 0.23 and 0.26 eV for 0 and 1 vol% DIO OSCs, respectively. The low reorganization energy indicates that more excitons can be separated into charges efficiently for devices incorporating 0.6 vol% DIO.[19] The theoretical energy of CT state (E_{CT}) is 1.36, 1.40 and 1.46 eV for devices incorporating 0, 0.6 and 1 vol% DIO, respectively, which are in good agreement with the empirical relation of $V_{oc} \approx E_{\mathrm{CT}}/q - 0.57$. Thus, the variation of V_{oc} about 0.1 V is correlated to the energy shift of

E_{CT} about 100 meV, which is influenced by the internal D/A interface inside the mesh network.

DIO shows a limited solubility of < 1 mg/mL to PTB7-Th but a high solubility of > 35 mg/mL to ITIC at room temperature (Table S4). Therefore, ITIC molecules removal from the bottom to the top surface of BHJ could be achieved when DIO is evaporated. To figure out the vertical distribution of PTB7-Th and ITIC in BHJ, the top and bottom surface molecular allocation of BHJ films was analyzed by measuring their physicochemical properties. As seen in Figure S7a, formamide droplets have the contact angle of 67˚ and 85˚ on top of ITIC and PTB7-Th films, respectively. For the top surface of PTB7-Th:ITIC blend films, the formamide contact angle decreased from 83˚ to 77˚ when DIO increased from 0 to 1 vol% with the trend to be gradually close to that of ITIC (67˚). Moreover, for the bottom surface of PTB7-Th:ITIC, the formamide contact angle increased from 71˚ to 79˚ when DIO increased from 0 to 1 vol% and was gradually closed to that of PTB7-Th (85˚). These results illustrate that ITIC molecules have migrated from the bottom to the top surface when DIO evaporated in low vacuum. Furthermore, surface energies of ITIC, PTB7-Th and BHJ solid films were measured based on Owens equation $\gamma_1(1+\cos\theta)=2(\gamma_s^D\gamma_1^D)^{1/2}+2(\gamma_s^P\gamma_1^P)^{1/2}$ (see details in the Table S5 and Table S6).[38] As displayed in Figure S7b, the surface energy of ITIC (30.9 mN/m) film is much higher than that of PTB7-Th (19.2 mN/m) film. Compared to pure PTB7-Th film, similar surface energy of PTB7-Th:ITIC (19.7 mN/m) film without DIO indicates PTB7-Th is rich on the surface of blend film for achieving a bulk free energy minimization. With increasing DIO content, the top surface energies reach up to 21.4 and 22.7 mN/m for 0.6 and 1 vol% DIO blend surface films, respectively. Oppositely, the bottom surface energies decreased from 27.2 to 21.2 mN/m when DIO increased from 0 to 1 vol% and were gradually close to that of PTB7-Th (19.2 mN/m). The tendency of surface energies of bottom and top films is in accordance with that of contact angles in different DIO volumes.

Since the neat PTB7-Th molecule does not contain nitrogen atoms whereas the neat ITIC molecule has nitrogen-containing components, the migration of ITIC can also be directly verified by X-ray photoelectron spectroscopy (XPS) measurements. According to the high-resolution XPS spectra of N 1s intensity of neat and blend films in **Figure 6**a, for blends the lowest and highest N 1s signals were detected on top film surfaces with 0 and 1 vol% DIO, respectively, indicating that ITIC molecules become rich on top surface of blends with the increase of DIO content. The XPS spectra of bottom surfaces are shown in Figure S7c. It demonstrates that bottom ITIC molecules are reduced with the increase of DIO from 0 to 1 vol%, which is contrary to the top surface law. The top and bottom XPS intensities of 0.6 vol% DIO blend film are located exactly in the middle among 0, 0.6 and 1 vol% DIO blend films, indicating the migration of ITIC molecules from bottom to top under the help of this amount of DIO additive is reasonable, which can be schematically depicted in Figure 6b. It is inferred from the above analysis that vast ITIC molecules deposited at the bottom of BHJ without DIO should be mainly attributed to the higher surface energy of pure ITIC compared to that of pure PTB7-Th.[10] The optimal vertical distribution of ITIC and PTB7-Th in BHJ was achieved by incorporating 0.6 vol% DIO, which is in accordance with PL, EL and FTPS spectra. However, redundant ITIC migrated to the top surface of BHJ employing superfluous 1 vol% DIO, resulting in ITIC accumulation on top surface. This can also be verified by the detected EL spectrum of ITIC in 1 vol% DIO device. The unfavorable enrichment of ITIC onto top surface leads to a low ITIC concentration in mixed domains, which reduces device current and fill factor. These results surprisingly agreed well with morphology and photophysics investigation.

The semilogarithmic plot of V_{oc} as a function of incident light intensity was measured, which shows a linear relationship with a slope of kT/q, as shown in Figure S8a. If the Shockley−Read−Hall (SRH) recombination is involved, a stronger dependence of V_{oc} on the light intensity with a slope greater than kT/q will be observed.[39-40] The dependence of V_{oc} on the light intensity for PTB7-Th:ITIC blend with incorporation of 0.6 vol% DIO showed a

slope of 1.06 kT/q, compared to 1.52 kT/q and 1.84 kT/q for blend films with 0 and 1 vol% DIO, respectively. It suggests that less SRH recombination involves under open-circuit condition for the 0.6 vol% DIO NF OSC than for other ratios of DIO NF OSCs. Furthermore, the light-intensity dependent J_{sc} measurement was also examined to verify the bimolecular recombination losses in the devices, as presented in Figure S8b. In general, the relationship between J_{sc} and incident light intensity (P_{light}) can be described as $J_{sc} \propto (P_{light})^{S}$. S should be equal to 1 if all dissociated free carriers are collected at the corresponding electrodes without charge recombination, while S < 1 indicates the presence of bimolecular recombination to some extent.[41-43] For the doctor-bladed PTB7-Th:ITIC film with incorporation of 0.6% DIO, S = 0.99 is obtained, compared to 0.94 and 0.92 for doctor-bladed PTB7-Th:ITIC blends with 0 and 1 vol% DIO, respectively. It indicates that the addition of 0.6 vol% DIO can sweep out charge carriers more efficiently with negligible bimolecular recombination compared to that of other ratios.[44]

Impedance spectroscopy (IS) was performed to investigate the effect of the DIO on the electrical properties of BHJ and interfaces in the doctor-bladed NF OSCs. [45-47] According to the device structure used, an equivalent circuit is defined as shown in Figure S9. The R_0 corresponds to the electrode resistance including ITO, ZnO, MoO_3 and Ag. The R_1 and C_1 correspond to BHJ layer. The R_2 and C_2 correspond to the two electrical contacts between ZnO/BHJ and BHJ/MoO_3. Figure S9 shows the combined curves of the resistance *vs* corresponding reactance, which are also called the Nyquist plot. Each element value is obtained as listed in Table S7. The OSC with 0.6 vol% DIO shows the smallest R_1 and the biggest C_1 among all doctor-bladed PTB7-Th:ITIC devices which is related to the finer D/A phase separation morphology. R_2 is increased and C_2 is decreased simultaneously when increasing DIO ratios, indicating ITIC-rich surface and ITIC-deficient bottom influence the contact electrical properties. Furthermore, the carrier transition time of this equivalent circuit

can be calculated from the equation $C_1 = \tau_{avg}/R_1$, where τ_{avg} is the average of the carrier transition time.[48] The longer τ_{avg} means the lower carrier recombination. It can be seen that τ_{avg} based on the 0.6 vol% DIO doctor-bladed NF OSC is longest in all devices (7.73E-06 s), confirming that the incorporation of appropriate DIO additive is favorable to improve the doctor-bladed PTB7-Th:ITIC device performance.

Laser beam induced current (LBIC) maps provide valuable insight into the spatial and local distribution of photocurrent, which contributes to determine whether the loss is occurring uniformly over the sample or locally in the case of pinhole formation or other reasons.[49-50] The observed variations in film morphologies and device characteristics are corroborated by LBIC measurements under 405 nm laser beam illumination, as shown in Figure S10. The doctor-bladed and spin-coated small area NF OSCs with 0.6 vol% DIO show the similar LBIC images without pronounced losses. However, the grievous losses and heterogeneities were occurred around the margin of the flexible ITO-free spin-coated large-area NF OSC (2.03 cm^2), which is in accordance with the worse *J-V* curve (Figure 2b). The flexible ITO-free doctor-bladed large-area NF OSC shows more uniform and higher current across the whole device compared to the spin-coated large-area counterpart, confirming that doctor-blading technique is suitable to NF OSCs manufacturing.

In conclusion, we demonstrated high-efficiency blade-printed fullerene-free OSCs with a PCE of 9.54%, which is the highest value up to date and is higher than its counterpart prepared by spin-coating. The enhancement of the photovoltaic performance was attributed to the favorable crystallinity, morphology and internal D/A structure realized through the addition of 0.6 vol% DIO. The migration of ITIC molecules from bottom to top helps form the optimal D/A interface distribution in BHJ, leading to the reduced exciton recombination and the optimized electrical parameters. The PCE of 7.6% also is one of the highest values reported to date among flexible ITO-free large-area single-junction nonfullerene OSCs,

contributing to the transition from lab-scale to fab-scale processed with R2R compatible doctor-blade printing.

Supporting Information

Supporting Information is available from the Wiley Online Library or from the author.

Acknowledgements

The authors are grateful to the NSFC Project (61774077, 61274062, 11204106), the Open Fund of the State Key Laboratory of Luminescent Materials and Devices (South China References University of Technology #2012-skllmd-10) and the Fundamental Research Funds for the Central Universities for financial support. Y.J. and F.Z. acknowledge funding from Swedish Research Council (VR 621-2013-5561) and China Scholarship Council (CSC) (No.201306730002) The collaboration between Linköping University and Jinan University is supported by Jinan University. T.P.R. were supported by the U.S. Office of Naval Research under contract N00014-15-1-2244. Portions of this research were carried out at beamline 7.3.3 and 11.0.1.2 at the Advanced Light Source, Molecular Foundry, and National Center for Electron Microscopy, Lawrence Berkeley National Laboratory, which was supported by the DOE, Office of Science, and Office of Basic Energy Sciences.

Received: ((will be filled in by the editorial staff))

Revised: ((will be filled in by the editorial staff))

Published online: ((will be filled in by the editorial staff))

[1] Z. C. He, C. M. Zhong, S. J. Su, M. Xu, H. B. Wu, Y. Cao, *Nat. Photonics* **2012**, 6, 591.

[2] R. Sondergaard, M. Hosel, D. Angmo, T. T. Larsen-Olsen, F. C. Krebs, *Mater. Today*

2012, 15, 36.

[3] C. J. M. Emmott, N. J. Ekins-Daukes, J. Nelson, *Energ. Environ. Sci*. **2014**, 7, 1810.

[4] a) F. C. Krebs, N. Espinosa, M. Hösel, R. R. Søndergaard, M. Jørgensen, *Adv. Mater.* 2014, 26, 29. b) F. Zhang, O. Inganäs, Y. Zhou, K. Vandewal, *Natl. Sci. Rev*. **2016**, 3, 222.

[5] J.-D. Chen, C. Cui, Y.-Q. Li, L. Zhou, Q.-D. Ou, C. Li, Y. Li, J.-X. Tang, *Adv. Mater.* **2015**, 27, 1035.

[6] J. Zhao, Y. Li, G. Yang, K. Jiang, H. Lin, H. Ade, W. Ma, H. Yan, *Nat. Energy* **2016**, 1, 15027.

[7] W. Zhao, S. Li, H. Yao, S. Zhang, Y. Zhang, B. Yang, J. Hou, *J. Am. Chem. Soc.* **2017**, 139, 7148.

[8] M. Jørgensen, J. E. Carlé, R. R. Søndergaard, M. Lauritzen, N. A. Dagnæs-Hansen, S. L. Byskov, T. R. Andersen, T. T. Larsen-Olsen, A. P. L. Böttiger, B. Andreasen, L. Fu, L. Zuo, Y. Liu, E. Bundgaard, X. Zhan, H. Chen, F. C. Krebs, *Sol. Energ. Mat. Sol. C.* **2013**, 119, 84.

[9] E. Bundgaard, F. Livi, O. Hagemann, J. E. Carlé, M. Helgesen, I. M. Heckler, N. K. Zawacka, D. Angmo, T. T. Larsen-Olsen, G. A. dos Reis Benatto, B. Roth, M. V. Madsen, M. R. Andersson, M. Jørgensen, R. R. Søndergaard, F. C. Krebs, *Adv. Energy* Mater. **2015**, 5, 1402186.

[10] Y. Lin, C. Cai, Y. Zhang, W. Zheng, J. Yang, E. Wang, L. Hou, *J. Mater. Chem. A* **2017**, 5, 4093.

[11] N. Li, D. Baran, G. D. Spyropoulos, H. Zhang, S. Berny, M. Turbiez, T. Ameri, F. C. Krebs, C. J. Brabec, *Adv. Energy Mater.* **2014**, 4, 1400084.

[12] D. Vak, K. Hwang, A. Faulks, Y.-S. Jung, N. Clark, D.-Y. Kim, G. J. Wilson, S. E. Watkins, *Adv. Energy Mater.* **2015**, 5, 1401539.

[13] H. Kang, G. Kim, J. Kim, S. Kwon, H. Kim, K. Lee, *Adv. Mater.* **2016**, 28, 7821.

[14] M. Helgesen, J. E. Carlé, G. A. dos Reis Benatto, R. R. Søndergaard, M. Jørgensen, E. Bundgaard, F. C. Krebs, *Adv. Energy Mater.* **2015**, 5, 1401996.

[15] F. Liu, S. Ferdous, E. Schaible, A. Hexemer, M. Church, X. Ding, C. Wang, T. P. Russell, *Adv. Mater.* **2015**, 27, 886.

[16] K. Zhao, H. Hu, E. Spada, L. K. Jagadamma, B. Yan, M. Abdelsamie, Y. Yang, L. Yu, R. Munir, R. Li, G. O. N. Ndjawa, A. Amassian, J. Mater. Chem. A **2016**, 4, 16036.

[17] N. Li, C. J. Brabec, *Energ. Environ. Sci.* **2015**, 8, 2902.

[18] X. Zhan, A. Facchetti, S. Barlow, T. J. Marks, M. A. Ratner, M. R. Wasielewski, S. R. Marder, *Adv. Mater.* **2011**, 23, 268. b) F. Zhang, M. Jonforsen, D. M. Johansson, M. R. Andersson, O. Inganas, *Synthetic Metals*, **2003**, 138, 555.

[19] W. Zhao, D. Qian, S. Zhang, S. Li, O. Inganas, F. Gao, J. Hou, *Adv. Mater.* **2016**, 28, 4734.

[20] L. Gao, Z. G. Zhang, H. Bin, L. Xue, Y. Yang, C. Wang, F. Liu, T. P. Russell, Y. Li, *Adv. Mater*. **2016**, 28, 8288.

[21] L. K. Jagadamma, M. Al-Senani, A. El-Labban, I. Gereige, N. Ndjawa, O. Guy, J. C. D. Faria, T. Kim, K. Zhao, F. Cruciani, *Adv. Energy Mater.* **2015**, 5, 1500204.

[22] J. E. Carlé, T. R. Andersen, M. Helgesen, E. Bundgaard, M. Jørgensen, F. C. Krebs, *Sol. Energ. Mat. Sol. C.* **2013**, 108, 126.

[23] P. Cheng, H. Bai, N. K. Zawacka, T. R. Andersen, W. Liu, E. Bundgaard, M. Jørgensen, H. Chen, F. C. Krebs, X. Zhan, *Adv. Sci.* **2015**, 2, 1500096.

[24] Y. Diao, Y. Zhou, T. Kurosawa, L. Shaw, C. Wang, S. Park, Y. Guo, J. A. Reinspach, K. Gu, X. Gu, B. C. Tee, C. Pang, H. Yan, D. Zhao, M. F. Toney, S. C. Mannsfeld, Z. Bao, *Nat. Commun.* **2015**, 6, 7955.

[25] X. Gu, Y. Zhou, K. Gu, T. Kurosawa, Y. Guo, Y. Li, H. Lin, B. C. Schroeder, H. Yan, F. Molina-Lopez, C. J. Tassone, C. Wang, S. C. B. Mannsfeld, H. Yan, D. Zhao, M. F. Toney, Z. Bao, *Adv. Energy Mater.* **2016**, 6, 1601225.

[26] Y. Lin, J. Wang, Z. G. Zhang, H. Bai, Y. Li, D. Zhu, X. Zhan, *Adv. Mater.* **2015**, 27, 1170.

[27] D. Angmo, M. Hösel, F. C. Krebs, *Sol. Energ. Mat. Sol. C.***2012**, 107, 329.

[28] Z. Peng, Y. Xia, F. Gao, K. Xiong, Z. Hu, D. I. James, J. Chen, E. Wang, L. Hou, *J. Mater. Chem. A* **2015**, 3, 18365.

[29] K. Liu, T. T. Larsen-Olsen, Y. Lin, M. Beliatis, E. Bundgaard, M. Jørgensen, F. C. Krebs, X. Zhan, *J. Mater. Chem. A* **2016**, 4, 1044.

[30] J. Zhang, Y. Zhao, J. Fang, L. Yuan, B. Xia, G. Wang, Z. Wang, Y. Zhang, W. Ma, W. Yan, W. Su, Z. Wei, *Small* **2017**, 13, 1700388.

[31] S. Berny, N. Blouin, A. Distler, H. J. Egelhaaf, M. Krompiec, A. Lohr, O. R. Lozman, G. E. Morse, L. Nanson, A. Pron, T. Sauermann, N. Seidler, S. Tierney, P. Tiwana, M. Wagner, H. Wilson, *Adv. Sci.* **2016**, 3, 1500342.

[32] S. Kim, H. Kang, S. Hong, J. Lee, S. Lee, B. Park, J. Kim, K. Lee, *Adv. Funct. Mater.* **2016**, 26, 3563.

[33] L. Nian, K. Gao, Y. Jiang, Q. Rong, X. Hu, D. Yuan, F. Liu, X. Peng, T. P. Russell, G. Zhou, *Adv. Mater.* **2017**, 4, 1700616.

[34] Y. Xia, C. Musumeci, J. Bergqvist, W. Ma, F. Gao, Z. Tang, S. Bai, Y. Jin, C. Zhu, R. Kroon, C. Wang, M. R. Andersson, L. Hou, O. Inganäs, E. Wang, *J. Mater. Chem. A* **2016**, 4, 3835.

[35] K. Tvingstedt, K. Vandewal, A. Gadisa, F. Zhang, J. Manca, O. Inganäs, *J. Am. Chem. Soc.* **2009**, 131, 11819.

[36] K. Vandewal, J. Widmer, T. Heumueller, C. J. Brabec, M. D. McGehee, K. Leo, M. Riede, A. Salleo, *Adv. Mater.* **2014**, 26, 3839.

[37] N. Li, J. D. Perea, T. Kassar, M. Richter, T. Heumueller, G. J. Matt, Y. Hou, N. S. Guldal, H. Chen, S. Chen, S. Langner, M. Berlinghof, T. Unruh, C. J. Brabec, *Nat. Commun.* **2017**, 8, 14541.

[38] D. K. Owens, Richmond, Virginia, R. C. Wendt, *J. Appl. Polym. Sci.* **1969**, 13, 1741.

[39] M. A. Uddin, T. H. Lee, S. Xu, S. Y. Park, T. Kim, S. Song, T. L. Nguyen, S.-j. Ko, S. Hwang, J. Y. Kim, H. Y. Woo, *Chem. Mater.* **2015**, 27, 5997.

[40] Y. Qin, M. A. Uddin, Y. Chen, B. Jang, K. Zhao, Z. Zheng, R. Yu, T. J. Shin, H. Y. Woo, J. Hou, *Adv. Mater.* **2016**, 28, 9416.

[41] G. Li, V. Shrotriya, J. Huang, Y. Yao, T. Moriarty, K. Emery, Y. Yang, *Nat. Mater.* **2005**, 4, 864.

[42] F. Huang, H. B. Wu, D. Wang, W. Yang, Y. Cao, *Chem. Mater.* **2004**, 16, 708.

[43] L. A. Perez, K. W. Chou, J. A. Love, T. S. van der Poll, D. M. Smilgies, T. Q. Nguyen, E. J. Kramer, A. Amassian, G. C. Bazan, *Adv. Mater.* **2013**, 25, 6380.

[44] C. Deibel, T. Strobel, V. Dyakonov, *Phys. Rev. Lett.* **2009**, 103, 036402.

[45] W. L. Leong, S. R. Cowan, A. J. Heeger, *Adv. Energy Mater.* **2011**, 1, 517.

[46] S. Yum, T. K. An, X. Wang, W. Lee, M. A. Uddin, Y. J. Kim, T. L. Nguyen, S. Xu, S. Hwang, C. E. Park, H. Y. Woo, *Chem. Mater.* **2014**, 26, 2147.

[47] K. Hess, Advanced theory of semiconductor devices, Wiley-IEEE Press, 2000.

[48] E.-P. Yao, C.-C. Chen, J. Gao, Y. Liu, Q. Chen, M. Cai, W.-C. Hsu, Z. Hong, G. Li, Y. Yang, *Sol. Energ. Mat. Sol. C.* **2014**, 130, 20.

[49] C. H. Peters, I. T. Sachs-Quintana, J. P. Kastrop, S. Beaupré, M. Leclerc, M. D. McGehee, *Adv. Energy Mater.* **2011**, 1, 491.

[50] a) F. C. Krebs, R. Søndergaard, M. Jørgensen, *Sol. Energ. Mat. Sol. C.* **2011**, 95, 1348. b) F. Zhang, K. G. Jespersen, C. Björström, M. Svensson, M.R. Andersson, V. Sundström, K. Magnusson, E. Moons, A. Yartsev and O. Inganäs, *Adv. Funct. Mater.* **2006**, 16, 667.

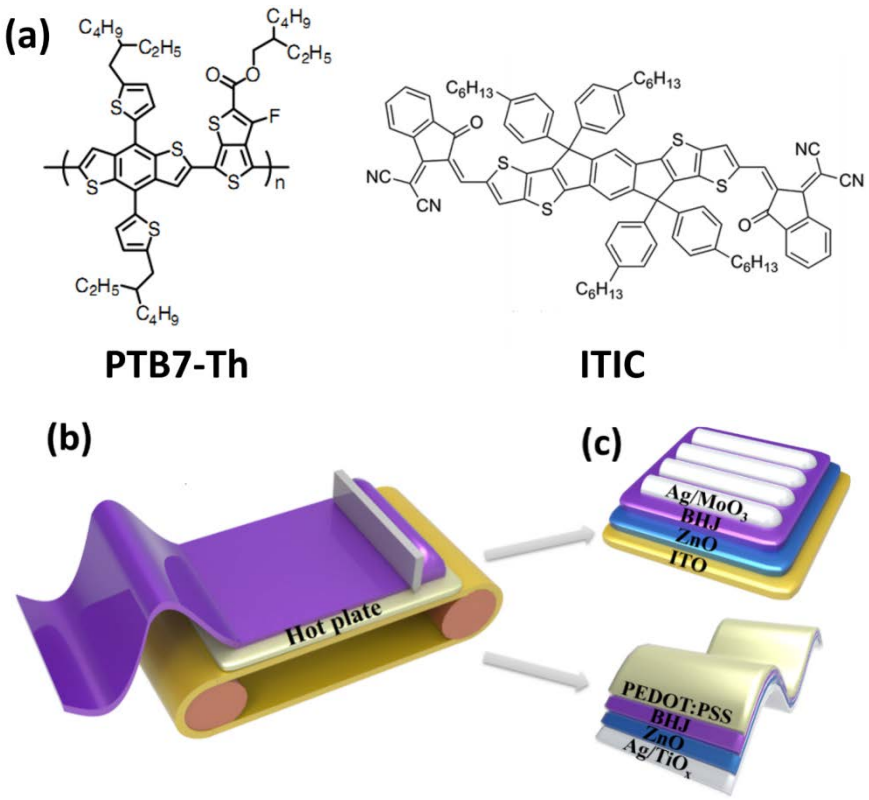

Figure 1. a) Chemical structures of donor PTB7-Th and nonfullerene acceptor ITIC. b) Doctor-blading fabrication process and c) Schematic of device architectures used in this study.

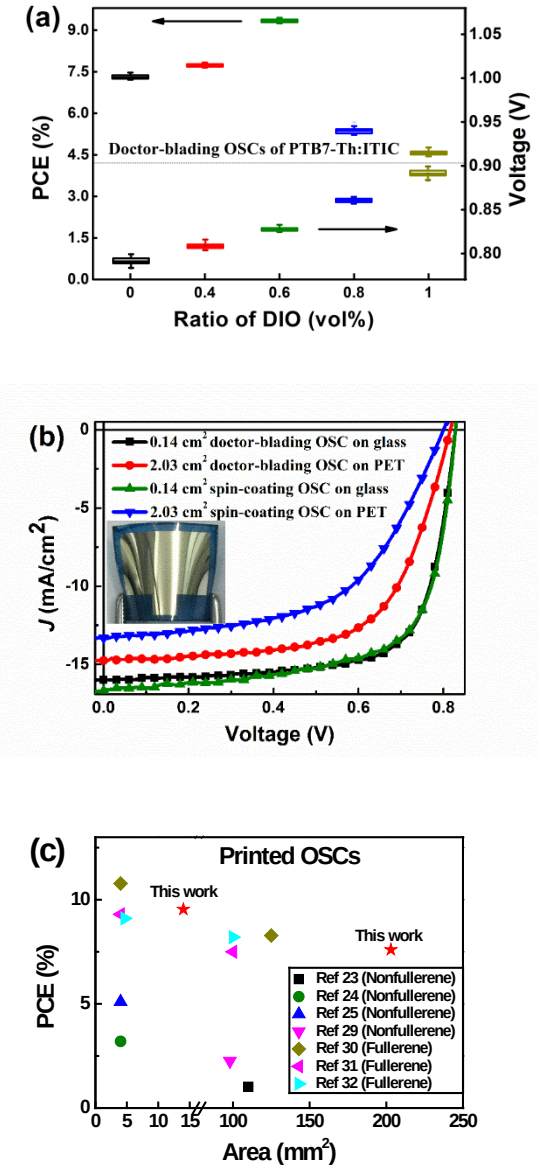

Figure 2. a) Corresponding statistical V_{oc} and PCE of doctor-blading OSCs with the increase volume of DIO. b) *J*–*V* curves of PTB7-Th:ITIC OSCs prepared by doctor-blading and spin-coating. The inset image is the photograph of doctor-blading ITO-free large-area flexible device. c) A comparison of the performance with previous reported printed NF and fullerence OSCs.[23-25, 29-32]

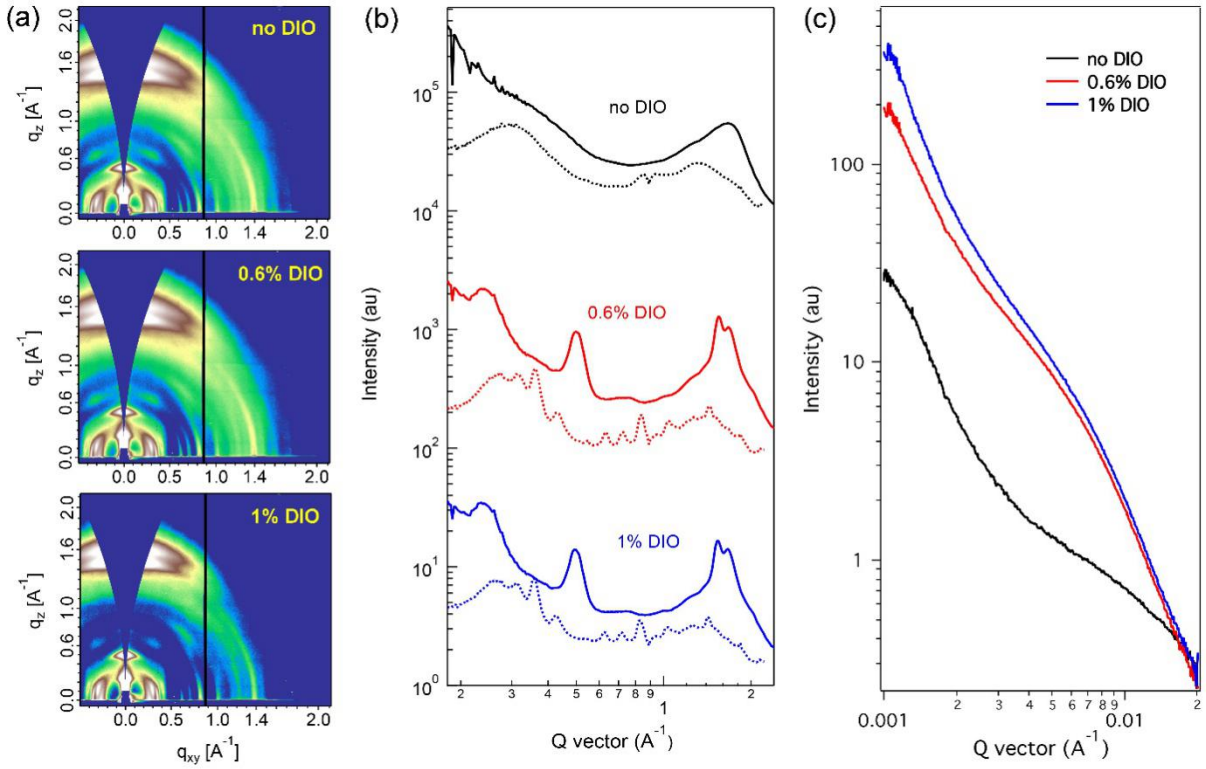

Figure 3. a) 2-D GIXD images of the NF blends with 0, 0.6 and 1 vol% DIO, respectively. b) In-plane (q_{xy}) (dotted line) and out-of-plane (q_z) (solid line) line cut profiles. c) Scattering intensity versus scattering vector plot for the three NF blends by RSoXS.

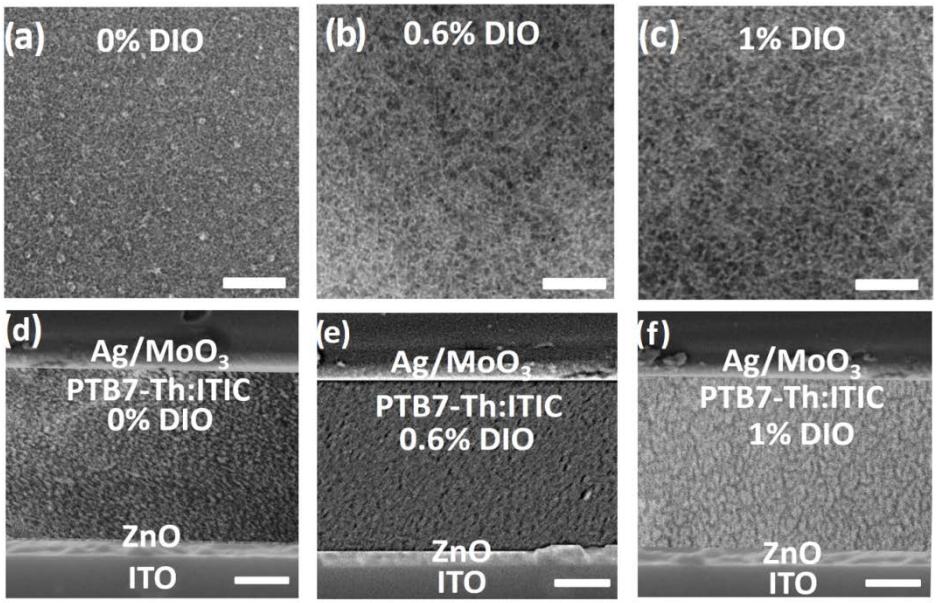

Figure 4. TEM images of doctor-bladed NF films and cross-sectional SEM images of by incorporatinga)-d) 0 vol%, b)-e) 0.6 vol% and c)-f) 1 vol% DIO, respectively (TEM bar = 100 nm, SEM bar = 50 nm).

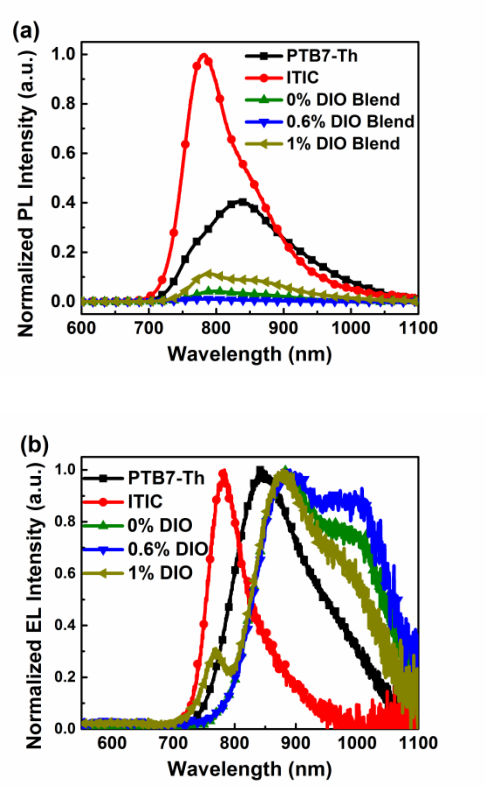

Figure 5. a) PL spectra of neat and blend films pumped by 405 nm light. b) Normalized EL spectra of the corresponding devices.

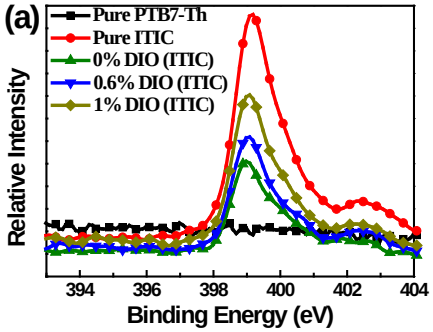

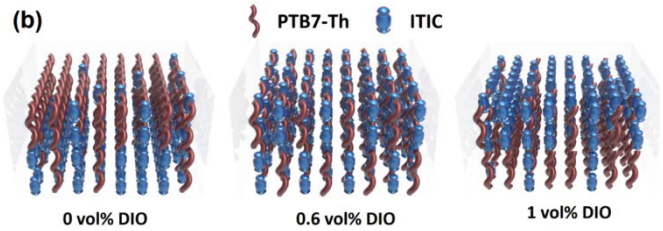

Figure 6. a) Relative N 1s XPS spectra of top surfaces of neat and PTB7-Th:ITIC blend films. b) A schematic diagram of PTB7-Th and ITIC distribution in BHJ. With the increase of DIO volume, ITIC molecules migrated from the bottom to the surface of BHJ.

Table 1. Photovoltaic parameters of PTB7-Th:ITIC OSCs by doctor-blade printing under illumination of AM 1.5G (100 mW/cm^2) in comparison to ones by spin-coating.

Active layer	Fabrication method	Ratio of DIO (%)	J_{sc} [mA/cm^2]	V_{oc} [V]	FF	PCE_{max} [%]
ITO-based Glass[a)]	Doctor-blading	0	15.3 (15.0)[b)]	0.79	0.62	7.47 (7.31)[c)]
		0.6	16.0 (15.6)	0.83	0.71	9.54 (9.33)
		1.0	11.5 (11.2)	0.89	0.47	4.79 (4.58)
	Spin-coating	0.6	16.7	0.83	0.68	9.31 (9.12)
ITO-free PET[d)]	Doctor-blading	0.6	14.7	0.81	0.63	7.60 (7.32)
	Spin-coating	0.6	13.3	0.80	0.55	5.86 (5.68)

[a)]The area of devices was 0.14 cm^2 based on the rigid glass. [b)]Data from EQE measurement (Figure S4). [c)]The average PCE was obtained from at least 20 devices. [d)]The area of devices was 2.03 cm^2 based on the flexible PET.

Printed nonfullerene organic solar cells (OSCs) are investigated with a power conversion efficiency of 9.54% via incorporating DIO additive for achieving a favorable nanoscale phase-separation. The migration of nonfullerene acceptor molecules from bottom to top helps form the optimal donor/acceptor interface distribution, leading to the reduced exciton recombination and optimized electrical parameters.

Keyword: doctor-blading nonfullerence organic solar cell, highest efficiency, large-area ITO-free flexible structure, processing additive, morphology

Yuanbao Lin, Yingzhi Jin, Sheng Dong, Wenhao Zheng, Junyu Yang, Alei Liu, Feng Liu, Yufeng Jiang, Thomas P. Russell, FengLing Zhang,* Fei Huang and Lintao Hou**

Printed Nonfullerene Organic Solar Cells with the Highest Efficiency of 9.5%